Biochimica et Biophysica Acta 1813 (2011) 1083–1091

Contents lists available at ScienceDirect

Biochimica et Biophysica Acta

journal homepage: www.elsevier.com/locate/bbamcr

The crystal structures of human S100B in the zinc- and calcium-loaded state at three pH values reveal zinc ligand swapping ☆

Thorsten Ostendorp [a], Joachim Diez [b], Claus W. Heizmann [c], Günter Fritz [d,*]

[a] Fachbereich Biologie, Mathematisch-Naturwissenschaftliche Sektion, Universität Konstanz, 78459 Konstanz, Germany
[b] Swiss Light Source (SLS) CH 5232 Villigen, Switzerland
[c] Division of Clinical Chemistry and Biochemistry, Department of Pediatrics, University Zürich, CH 8032 Zürich, Switzerland
[d] Department of Neuropathology, University of Freiburg, 79106 Freiburg, Germany

ARTICLE INFO

Article history:
Received 22 July 2010
Received in revised form 4 October 2010
Accepted 4 October 2010
Available online 13 October 2010

Keywords:
S100 protein
S100B
EF-hand
Crystallography
Calcium
Zinc
Copper

ABSTRACT

S100B is a homodimeric zinc-, copper-, and calcium-binding protein of the family of EF-hand S100 proteins. Zn^{2+} binding to S100B increases its affinity towards Ca^{2+} as well as towards target peptides and proteins. Cu^{2+} and Zn^{2+} bind presumably to the same site in S100B. We determined the structures of human Zn^{2+}- and Ca^{2+}-loaded S100B at pH 6.5, pH 9, and pH 10 by X-ray crystallography at 1.5, 1.4, and 1.65 Å resolution, respectively. Two Zn^{2+} ions are coordinated tetrahedrally at the dimer interface by His and Glu residues from both subunits. The crystal structures revealed that ligand swapping occurs for one of the four ligands in the Zn^{2+}-binding sites. Whereas at pH 9, the Zn^{2+} ions are coordinated by His15, His25, His 85′, and His 90′, at pH 6.5 and pH 10, His90′ is replaced by Glu89′. The results document that the Zn^{2+}-binding sites are flexible to accommodate other metal ions such as Cu^{2+}. Moreover, we characterized the structural changes upon Zn^{2+} binding, which might lead to increased affinity towards Ca^{2+} as well as towards target proteins. We observed that in Zn^{2+}–Ca^{2+}-loaded S100B the C-termini of helix IV adopt a distinct conformation. Zn^{2+} binding induces a repositioning of residues Phe87 and Phe88, which are involved in target protein binding. This article is part of a Special Issue entitled: 11th European Symposium on Calcium.

S100B is a small (10.7 kDa) Zn^{2+}- and Ca^{2+}-binding EF-hand protein that is highly expressed in astrocytes [1] and constitutes with 0.5% one of the most abundant soluble proteins in brain. It is a member of the S100 protein family, which represents with 21 members the largest subgroup in the EF-hand protein superfamily [1,2] as well as larger multimers. We recently identified and structurally characterized tetra-, hexa-, and octameric species of S100B [3] as well as larger multimers. Further multimers are reported for S100A12 and S100A8/A9 heterodimer. S100B is involved in cellular processes such as cell growth, cell cycle control [4], and differentiation [5]. Intracellularly, S100B binds in Ca^{2+}-dependent manner to cytoskeletal proteins such as annexin II, tubulin filaments, or CapZ [1,2]. Moreover, it is involved in the regulation of metabolic enzymes like aldolase [6] and glycogen phosphorylase [7]. S100B transfers the Ca^{2+} signal into phosphorylation status by interaction with kinases such as NDR-kinase [8] or interaction with proteins regulated by phosphorylation like transcription factor p53 [9] and microtubule-associated tau protein [10]. In addition to its intracellular function as Ca^{2+} sensor S100B is secreted to the extracellular space where it exhibits cytokine-like functions. It was shown that S100B is secreted by vesicular transport from gliablastoma cells upon changes in intracellular Ca^{2+} or Zn^{2+} levels [11]. Once secreted, S100B exerts dose dependent neurotrophic [12,13] or neurotoxic action [13]. Altered expression levels of S100B are associated with neurodegenerative disorders like Alzheimer's disease [14,15] and cancer [1,16].

Besides Ca^{2+}, several S100 proteins bind Zn^{2+} with high affinity. The different Zn^{2+}-binding S100 proteins can be sorted into two groups. Members of the first group bind Zn^{2+} via Cys residues and comprise S100A2 [17], S100A3 [18,19], S100A4 (Koch et al., unpublished results), and S100A6 [20], whereas members of the second group like S100A7, S100A8/A9, S100A12, and S100B coordinate Zn^{2+} only with residues Asp, His, or Glu. In contrast to Cys, these residues cannot undergo redox reactions and are also suited to coordinate the redox labile Cu^{2+}. In fact, several S100 proteins are reported to bind Cu^{2+} with high affinity [20–23]. The structures of S100A12 in complex with Cu^{2+} [20] or Zn^{2+} [24] illustrate that the metal ions bind to identical sites suggesting that the other Zn^{2+}-binding S100 proteins display similar flexibility with regard to nature of the bound metal ion. This flexibility to accommodate different metal ions must be reflected in specific structural properties of the site. So far structural information is available from the crystal

Abbreviations: PEG, Polyethylenglycol; CD, circular dichroism

☆ This article is part of a Special Issue entitled: 11th European Symposium on Calcium.

* Corresponding author. Department of Neuropathology, University of Freiburg, Breisacher Str. 64, 79106 Freiburg, Germany. Tel.: +49 761 270 5078; fax: +49 761 270 5050.
E-mail address: guenter.fritz@uniklinik.freiburg.de (G. Fritz).

0167-4889/$ – see front matter © 2010 Published by Elsevier B.V.
doi:10.1016/j.bbamcr.2010.10.006

structure of S100A7 with one Zn^{2+} ion bound [20], the solution structure rat S100B in the Ca^{2+}–Zn^{2+}-loaded state [25], the crystal structure of Ca^{2+}–Zn^{2+}-loaded state [20] and from the X-ray structures of bovine Ca^{2+}–Zn^{2+}-loaded S100B [26], Ca^{2+}–Cu^{2+}-loaded S100A12, the Cu^{2+} binding to the Zn^{2+} sites [20]. S100B binds Zn^{2+} with higher affinity than Ca^{2+}. Zn^{2+}-binding affinities of 20 nM and 100 nM were determined by fluorescence titrations for bovine S100B [27] and by isothermal calorimetry for rat S100B [28], respectively. It was shown that Zn^{2+} binding to S100B increases its affinity towards Ca^{2+} [27] as well as towards peptides derived from target proteins [29–32]. The structures of Ca^{2+}–Zn^{2+}-loaded S100B from rat determined by multidimensional NMR spectroscopy and Ca^{2+}–Zn^{2+}-loaded S100B from bovine by X-ray crystallography revealed that two Zn^{2+} ions bind per homodimer [26,32] at a site similar to the Cu^{2+}-binding site in S100A12 [20]. At neutral pH, the Zn^{2+} ions are coordinated by three His and one Glu residues originating from both subunits in the homodimeric protein. However, spectroscopic data on Cu^{2+}-loaded S100B revealed that Cu^{2+} is coordinated by four equivalent N atoms originating most likely from four histidine residues [21] (Koch, M., Ostendorp, T., Antholine, W.A., Kroneck, P.M.H., Fritz, G. publication in preparation), suggesting some flexibility of the site in S100B. In order to get detailed structural information on this versatile metal ion binding site in S100B and the structural changes upon accompanied with metal ion binding, we determined the structure of human Ca^{2+}–Zn^{2+}-loaded S100B at three different pH values by X-ray crystallography. We report here on three high-resolution crystal structures of Zn^{2+}–Ca^{2+}-loaded human S100B exhibiting a flexible Zn^{2+}-binding site and structural changes, which might lead to an increased affinity towards target proteins.

1. Materials and methods

1.1. Crystallization

Recombinant dimeric human S100B was expressed and purified as described previously [33]. S100B in 10 mM Tris–HCl pH 7.6 was concentrated by ultrafiltration to 10 mg ml^{-1} (0.46 mM dimer) and 10 mM $CaCl_2$, 0.92 mM $ZnCl_2$ were added. Crystallization trials were performed by the sitting-drop vapor diffusion method mixing 2 µl drops of protein solution with 2 µl out of 500 µl reservoir. Diffracting crystals were obtained with 0.1 M MES pH 6.5 21% PEG5000MME, or 0.05 M TAPS pH 9.0, 30% PEG4000, or 0.05 M CAPS pH 10.0, 23% PEG5000MME as precipitant. The crystals grew within 2–4 weeks at 16 °C (at pH 6.5) or 18 °C (at pH 9.0 and pH 10.0). Crystals grown at pH 6.5 and pH 10 belonged to the space group $P2_1$ or when grown at pH 9.0 to the space group $C222_1$. The crystals were immersed for 5 s in cryo-protectant solution prior data collection and flash-frozen in the cryo-nitrogen stream. The cryo-protectant solution contained 0.1 M MES pH 6.5, 33% PEG5000MME, 0.02 M TAPS pH 9.0 32% PEG4000, and 0.02 M CAPS pH 10.0 30% PEG5000 MME, respectively.

1.2. Spectroscopy

Far UV CD spectra of S100B were recorded with a spectropolarimeter J-715 (Jasco) in 0.10- and 0.01-cm quartz cells at 20 °C. The protein concentration was 5 µM in 20 mM Tris-Cl, pH 7.5. Six spectra of protein were recorded between 260 and 180 nm, averaged and corrected for the buffer spectrum. Difference spectra were calculated from dilution corrected spectra of metal-ion-loaded S100B and apo-S100B. UV–Vis spectra of Co^{2+} substituted S100B were recorded in 1-cm quartz cells under exclusion of dioxygen with a Cary3 (Varian) spectrophotometer at 20 °C. Protein concentration was 285 µM in 20 mM Tris–Cl, pH 7.6. Divalent metal ions were removed from all buffers by Chelex (Bio-Rad) treatment.

1.3. X-ray data collection

Data sets were collected using synchrotron radiation at the Swiss Light Source (SLS) beamline X06SA equipped with a MAR225 CCD detector at 100 K. All data were scaled and processed using the program package XDS [34,35]. Crystal parameters and data collection statistics are listed in Table 1.

1.4. Structure determination and crystallographic refinement

The structure of human Ca^{2+}–Zn^{2+}-loaded S100B was solved by molecular replacement by CNS [36] and MOLREP [37]. The subunits A and B of the human Ca^{2+}–S100B served as a search model [38]. The model was refined with REFMAC5 [39] implemented in the CCP4 package [40]. Assignment of TLS groups for refinement was done by TLSMD server [41]. Solvent positions were determined using ARP/wARP [42]. Repeated cycles of manual rebuilding of the models were done after each refinement step with the programs O [43] and Coot [44]. The quality and geometry of the structures were evaluated by PROCHECK [45]. Illustrations and structural alignments were prepared using the program Pymol [46]. The coordinates and structure factors have been submitted to the Protein Data Bank with accession codes 3DOY, 3CZT, and 3D10.

Table 1
Data collection and refinement statistics.

Crystallization pH	pH 6.5	pH 9.0	pH 10.0
Space group	$P2_1$	$C222_1$	$P2_1$
Unit cell parameters (Å)	$a=34.89$, $b=58.15$	$a=34.95$, $b=89.26$	$a=34.75$, $b=58.18$
	$c=47.66$	$c=59.58$	$c=47.85$
	$\alpha=\gamma=90°$, $\beta=111.12°$	$\alpha=\beta=\gamma=90°$	$\alpha=\gamma=90°$, $\beta=111.08°$
Resolution	13–1.50 (1.6–1.5)	18–1.40 (1.55–1.4)	44–1.65 (1.75–1.65)
Completeness (%)	97.0 (93.4)	97.0 (89.2)	98.6 (95.8)
No. of unique reflections	27707 (4677)	18236 (4340)	21394 (3392)
Redundancy	3.8 (3.4)	5.8 (2.9)	3.5 (3.0)
R_{merge} (%)	7.7 (51.7)	5.2 (21.3)	5.3 (29.0)
$I/\sigma(I)$	8.5 (2.3)	18.4 (5.1)	13.5 (3.5)
SU per asymmetric unit	2	1	2
R_{cryst} (%)	20.5 (26.3)	16.1 (19.3)	20.9 (25.6)
R_{free}[a] (%)	25.9 (34.0)	22.1 (28.0)	27.5 (33.6)
RMS deviation from ideal geometry:			
Bond distances (Å)	0.015	0.019	0.021
Bond angles (degree)	1.52	1.49	1.90

The numbers in parentheses are the statistics for the highest resolution shell.
[a]R_{free} was calculated against 5% of the total reflections omitted from the refinement.

Table 2
Interhelical angles and distances of $Zn^{2\pm}$–$Ca^{2\pm}$–S100B structures and compared to other S100 structures.

	Interhelical angle (degrees)			Interhelical distances (Å)		
	I–II	II–III	III–IV	I–II	II–III	III–IV
[1]Human Zn–Ca–S100B, pH 6.5	137	100	106	15.5	11.6	15.7
[2]Human Zn–Ca–S100B, pH 9	138	100	107	15.4	11.8	15.0
[3]Human Zn–Ca–S100B, pH 10	138	101	106	15.4	11.7	15.0
[4]Human Ca–S100B (pH 7.5)	135	101	104	15.1	11.8	15.7
[5] Bovine Ca–S100B, (pH 7.5)	135	101	103	15.2	11.9	15.6
[6]Rat Zn–Ca–S100B (NMR pH 7.2)	130	129	140	14.6	11.0	8.5
[7]Bovine Zn–Ca–S100B (X-ray pH 7.2)	137	100	103	14.7	11.7	15.4
[8]Human Cu–Ca–S100A12	142	107	120	14.2	11.3	15.7
[9]Human Zn–Ca–S100A7	138	127	130	16.0	11.3	14.0

[1](3DOY), [2](3CZT), [3](3D10) this study, [4](2 H61) , [5](1MHO) [64], [6](1XYD) [32], [7](3CR2) [26], [8](1ODB) [20], [9](2PSR) [25]. Helices were assigned using DSSP [65]; helix I was defined as residues 2–18; helix II, residues 29–39; helix III, residues 51–60; and helix IV, residues 70–87.

2. Results and discussion

2.1. Crystallization and refinement

The protein crystallized only in the presence of equimolar amounts of Zn^{2+} and excess amounts of Ca^{2+}. Addition of excess of Zn^{2+} led to precipitation of the protein. Crystals grown in space group $P2_1$ contained one dimer per asymmetric unit, whereas the crystal grown at pH 9.0 belonged to space group $C222_1$ and contained only one subunit per asymmetric unit. In this case, the full dimer was obtained by crystallographic symmetry operations. The crystals obtained at pH 6.5 and 10.0 diffracted to 1.6 and 1.5 Å resolution and were refined using 4 TLS groups for each subunit resulting in $R_{cryst} = 20.5$ ($R_{free} = 25.9$) and $R_{cryst} = 20.9$ ($R_{free} = 27.5$), respectively. Crystals grown at pH 9.0 diffracted to 1.4 Å and the structure and individual anisotropic B-factor refined for all atoms. Including hydrogen atoms in riding positions in the last cycles of refinement resulted in a drop of 0.9% in R_{cryst} and 1.5% in R_{free} to final R_{cryst} of 16.1% and R_{free} of 22.1%.

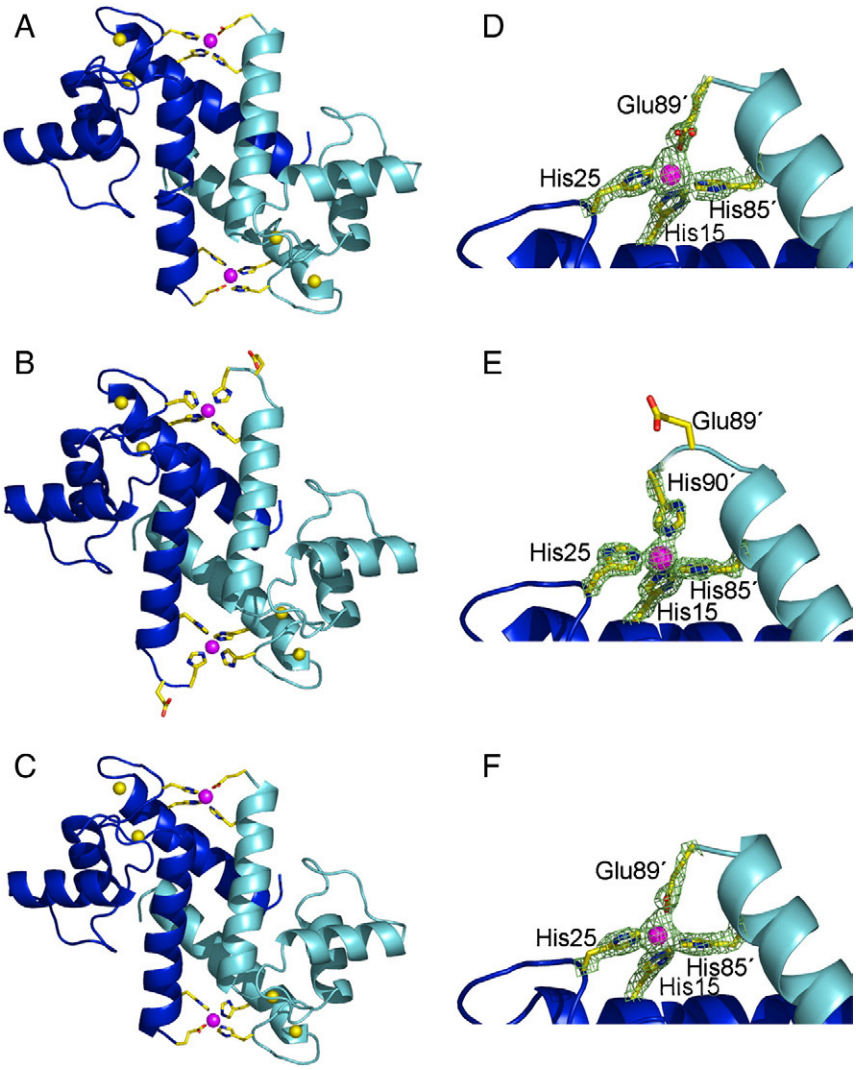

Fig. 1. Overall structure of $Zn^{2\pm}$–$Ca^{2\pm}$-loaded S100B and structure $Zn^{2\pm}$-binding sites. Overall structure of S100B dimer at different pH values. (A) at pH 6.5, (B) at pH 9.0, and (C) at pH 10.0. The Zn^{2+} coordinating residues (His and Glu) are shown in stick type. The subunits are colored in blue and cyan. Ca^{2+} ions are shown as yellow spheres, Zn^{2+} ions are shown as magenta spheres. The overall fold and the location of the Zn^{2+}-binding site are very similar in all three structures. (D) Zn^{2+}-binding site at pH 6.5. The Zn^{2+} is coordinated tetrahedrally by His15(Nε); His25(Nε) from one subunit and by His85′(Nε) and Glu89′ from the second subunit. (B and E) The Zn^{2+}-binding site at pH 9.0, the Zn^{2+} ion is coordinated by His15; His25, His85′, and His90′. Glu89′ that is coordinating Zn^{2+} at pH 6.5 and 10.0 is shown in stick type. Coordination by His90′ leads to a reorientation of Glu89′ pointing with its side chain to the opposite direction of the Zn^{2+}-binding site. (F) Zn^{2+}-binding site of S100B at pH 10. The Zn^{2+} ion is coordinated by His15 His25, His85′, and Glu89′. The electron density around the coordinating residues and the Zn^{2+} ions is shown in green at 1.5σ.

Table 3
Table 2: zinc–ligand distances

Zn to ligand	pH 6.5[a]	pH 9.0	pH 10.0[a]
His15 NE2 (Å)	2.00 ± 0.02	2.07	2.11 ± 0.06
His25 NE2 (Å)	1.95 ± 0.04	1.86	1.90 ± 0.05
His85 NE2 (Å)	2.16 ± 0.02	2.13	2.15 ± 0.03
His90 NE2 (Å)	–	1.88	–
Glu89 OE (Å)	1.98 ± 0.05	–	2.46 ± 0.18

[a] Mean distances and standard deviations of both Zn^{2+} sites in S100B homodimer.

The somewhat higher *R* values for the structures at pH6.5 and pH 10.0 might be a result of the less ordered C-terminus compared to the structure at pH 9.0. In the structure at pH 9.0, the Zn^{2+} is coordinated in the fourth position by His90, whereas in the other two structures, Glu89 is coordinating. The coordination by His90 leads to a higher ordered C-terminus that could be modeled better resulting in lower *R*-factors. For details, see Table 1.

The packing of S100B molecules is very similar in both crystal forms although crystals of at pH 6.5/pH 10 belong to a different space group than crystals grown at pH 9.0. Closer inspection of the symmetry axis shows that in the crystals grown at pH 9.0 the intrinsic twofold symmetry axis of the S100B homodimers is a true crystallographic axis. Therefore, the same axis exists in the lower symmetry space group $P2_1$ as well as in the higher symmetry space group $C222_1$ without affecting packing.

2.2. Overall structure

Zn^{2+}–Ca^{2+}-loaded S100B is a homodimeric heart-shaped molecule stabilized by hydrophobic interactions between the two subunits. The overall fold of Zn^{2+}–Ca^{2+}–S100B is very similar to that of Ca^{2+}-loaded S100B or other dimeric Ca^{2+}-loaded S100 proteins. Each subunit comprises two helix–loop–helix EF-hand motifs connected by a further loop. All three structures at pH values of pH 6.5, 9, and 10 revealed two Zn^{2+} ions and four Ca^{2+} ions bound per homodimer. The relative height of the anomalous signals for Zn^{2+} and Ca^{2+} ions showed that all metal-ion binding sites are fully occupied. The three structures of Zn^{2+}–Ca^{2+}–S100B show a very similar fold as illustrated by RMSDs for the Cα (residues 1–89) positions of approximately 0.2 Å and by the interhelical angles and distances (helix pair I–II = 138 ± 1°, 15 Å; helix pair III–IV = 106 ± 1°, 15 Å, see also Table 2). Thus, the overall fold of Zn^{2+}–Ca^{2+}–S100B does not change in a pH range from 6.5 to 10.0 (Fig. 1A–C). Nevertheless, variation in the type of Zn^{2+} coordination occurs in the different structures. In the following, we will compare the structures obtained at the three different pH values. In order to differentiate the structures, we will use the different pH values as an assignment.

2.3. Structure of the Zn^{2+}-binding sites exhibit ligand swapping

In all three structures, the two Zn^{2+} ions in S100B dimer are coordinated in a distorted tetrahedron by residues from both subunits (Fig. 1D–F). In the structures obtained at pH 6.5 and pH 10, histidines His15, His25 from one subunit and His85′ and a Glu89′ from the second subunit serve as ligands (Fig. 1D, F). The same ligands have been identified in rat and bovine Zn^{2+}–Ca^{2+}–S100B determined at pH 7.2 [26,32]. In contrast to these structures in Zn^{2+}–Ca^{2+}–S100B at pH 9, the Zn^{2+} ions are coordinated by the four histidines His15, His25, His85′, and His90′ (Fig. 1E). This type of coordination is in agreement with the observed coordination of Cu^{2+} in S100B

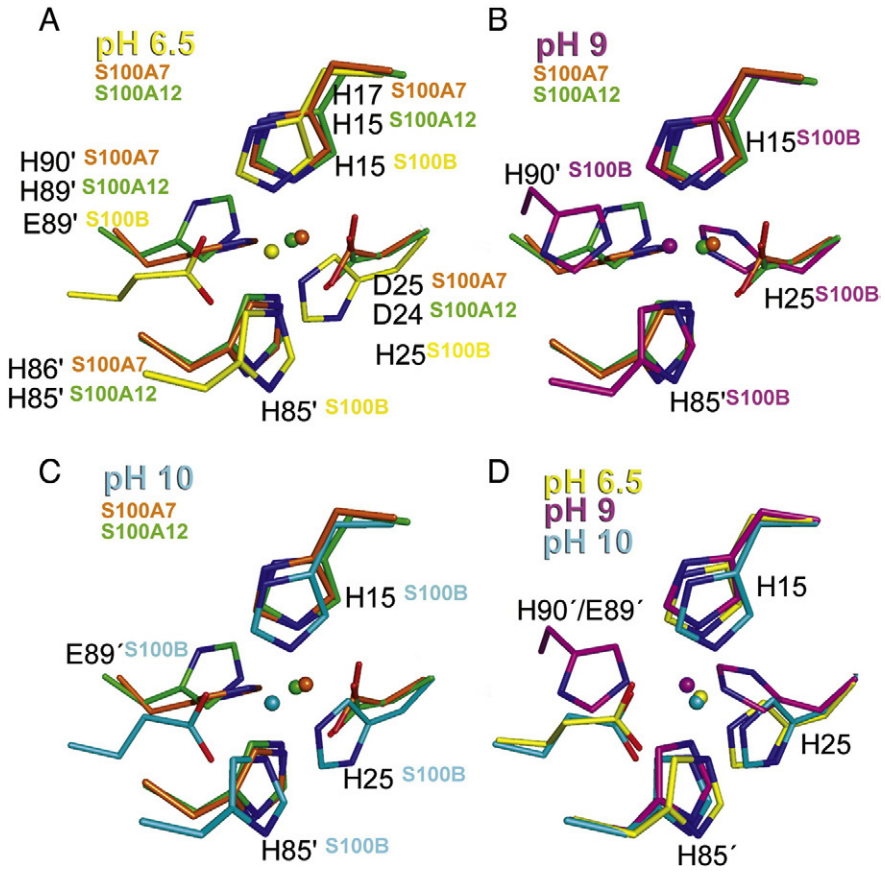

Fig. 2. Comparison of Zn^{2+}-binding sites in S100B with Zn^{2+}/Cu^{2+}-binding sites of S100A7 and S100A12. Residues of Zn^{2+}-binding site in S100B at pH 6.5 (yellow) (A), pH 9.0 (magenta) (B), and pH 10.0 (cyan) (C) in superposition with Zn^{2+}/Cu^{2+}-binding sites of S100A7 (orange, pdb code 2PSR) and S100A12 (green, pdb code 1ODB). (D) Superposition of Zn^{2+}-binding sites in S100B determined in this study. The ions are shown as spheres, yellow/magenta/cyan is for the S100B Zn^{2+} ions, S100A7 Zn^{2+} ion is in orange, and S100A12 Cu^{2+} ion is in green.

determined by EPR spectroscopy [21]. The ligand swapping probably enables S100B to accommodate further metal ions such as Cu^{2+}, which prefers nitrogen over oxygen coordination and contributes to functional flexibility of S100B. All histidine residues coordinate Zn^{2+} via the imidazole Nε atom. Zn^{2+}–ligand distances were not fixed during refinement in order to get an unbiased view of the Zn^{2+}-binding site. The Zn^{2+} to nitrogen and oxygen distances vary in a certain range but are in agreement with previously observed Zn^{2+}–ligand distances in proteins [47] (for details, see Table 3).

A similar type of coordination has been shown for Cu^{2+} in the Cu^{2+}–Ca^{2+}-loaded S100A12 (His15, His85′ and His89′, and Asp25, Fig. 2A–C) [20] and for the Zn^{2+}-loaded S100A7 (His15, His85′ and His89′, and Asp25, Fig. 2A–C). In the case of Cu^{2+}–Ca^{2+}–S100A12, the coordinating Asp25 corresponds to His25 in S100B. There is no flexibility in this position of the coordination, which might lead to a somewhat lower affinity towards Cu^{2+} in S100A12 than in S100B. Sequence alignments suggest that this Zn^{2+}/Cu^{2+}-binding motif is conserved in S100A8 and S100A9 and homologous S100 proteins from different species[20]. Noteworthy, S100B, S100A7, S100A8/A9, and S100A12 proteins occur in the extracellular space, where they act as cytokines [48,49]. Other Zn^{2+}-binding proteins such as S100A2, S100A3, or S100A6 bind Zn^{2+} via Cys residues and occur predominantly intracellularly. Extracellularly, Cys residues are prone to oxidation and readily form disulfides, which would abolish Zn^{2+} binding. The Zn^{2+}-binding sites in S100B, S100A7, S100A8/A9, and S100A12 built by His and Asp/Glu residues are redox-insensitive and stay functional in the extracellular space, suggesting that Zn^{2+} binding is important for their cytokine-like function.

2.4. Conformational changes induced by Zn^{2+} binding

Alignment of structures of human Ca^{2+}–Zn^{2+}–S100B with human Ca^{2+}–S100B (subunits AB, pdb code 2H61) showed that Zn^{2+} binding did not induce major conformational changes (Fig. 3). Nevertheless, a small but significant change was observed for the conformation of the C-terminal classical EF-hand. The interhelical angles in Zn^{2+}–Ca^{2+}–S100 increased 2–3° compared to Ca^{2+}–S100B. This finding suggests that Zn^{2+} binding to Ca^{2+}-loaded human S100B induces a more open conformation. These changes in interhelical angle are accompanied by rearrangements in the C-terminus involved in target protein binding. Comparison of human Zn^{2+}–Ca^{2+}–S100B with the structures Ca^{2+}–S100B determined by NMR or X-ray crystallography shows that the flexible C-terminal region following helix IV adopts a distinct conformation. Additional main chain hydrogen bonds are observed, e.g., between the carbonyl oxygen of His85 and amide nitrogen of Phe88, as well as between carbonyl oxygen of Glu86 and amide nitrogen of Phe89 corresponding to a small elongation of helix IV.

To test whether Zn^{2+} binding to Ca^{2+}–S100B induces a change in secondary structure content in solution, CD spectra of apo-S100B, Zn^{2+}–S100B, Ca^{2+}–S100B, and Zn^{2+}–Ca^{2+}–S100B were compared. Addition of Ca^{2+} or Zn^{2+} leads to a small decrease in ellipticity around 222 nm. Addition of Zn^{2+} to Ca^{2+}–S100B caused a further decrease around 222 nm (Fig. 4). Such a decrease in ellipticity at 222 nm is consistent with an increase of the α-helical content in S100B by ca. 4 residues [50]. The changes in the CD around 222 nm are also consistent with a change in interhelical angles [51], which was observed in the structure of Zn^{2+}–Ca^{2+}–S100B. In summary, the CD spectra of S100B in solution corroborate with the structural changes observed in the crystal. Noteworthy, sole Zn^{2+} binding to S100B leads like Ca^{2+} binding to an exposure of hydrophobic patches to the solvent [52] and can mediate Ca^{2+}-independent interactions with target proteins [31,53] or interaction with hydrophobic matrices [54]. These observations as well as the CD difference spectra suggest that sole binding of Zn^{2+} induces structural changes resembling those upon Ca^{2+} binding. However, it is rather unlikely that the conformational changes are due to Zn^{2+} binding to the EF-hands. The residues

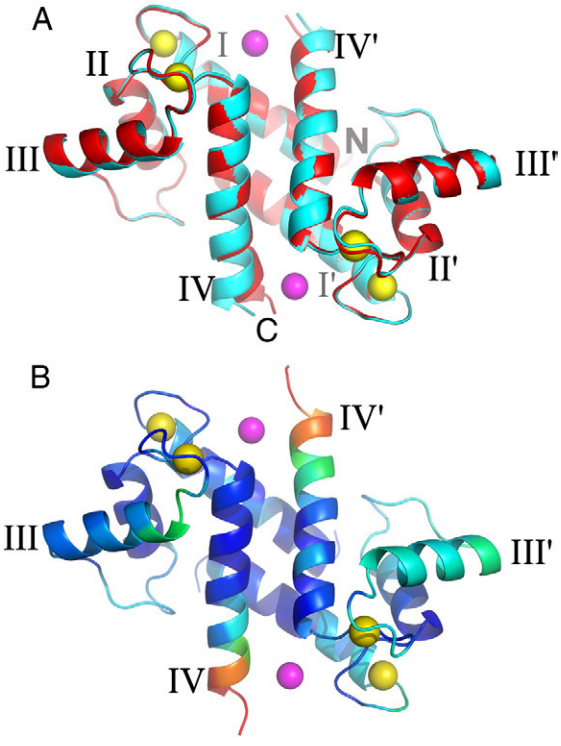

Fig. 3. Comparison of $Zn^{2\pm}$–$Ca^{2\pm}$–S100B with $Ca^{2\pm}$–S100B. (A) Structural alignment of human Zn^{2+}–Ca^{2+}–S100B (cyan) human Ca^{2+}–S100B (red; pdb entry 2 H61, chains AB). Both structures are shown as cartoons and bound Zn^{2+} and Ca^{2+} ions are shown as spheres in magenta and yellow, respectively. The superposition illustrates the similarity of both structures. (B) In order to illustrate the changes induced by Zn^{2+} binding, the RMSD between Zn^{2+}–Ca^{2+}–S100B and Ca^{2+}–S100B is shown as color code mapped onto the protein structure of Zn^{2+}–Ca^{2+}–S100B: blue, deviations between 0.1 and 0.3 Å; light blue cyan, 0.4–0.6 Å; green, 0.7–1.0 Å; orange–red, ≥ 1.1 Å. The largest changes in the structure are observed at the C-terminus of helix IV. Further deviations are observed for the position of helix III, which is also illustrated by changes in the interhelical angle between helix II and IV (see also Table 2). (C) Superposition of human Zn^{2+}–Ca^{2+}–S100B (cyan) of this study with rat Zn^{2+}–Ca^{2+}–S100B determined by NMR.

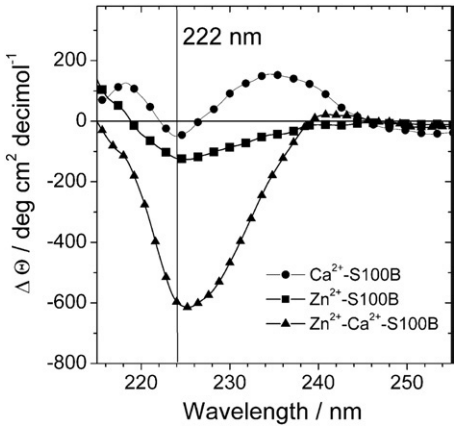

Fig. 4. Far UV CD spectra of $Ca^{2\pm}$- and $Zn^{2\pm}$-bound S100B. CD difference spectra of S100B after addition of Ca^{2+} (1 mM), Zn^{2+} (1 equivalent), and Ca^{2+}/Zn^{2+}. Addition of Ca^{2+} (line with circles) leads only to a slight decrease in ellipticity at 222 nm, which indicates a minor increase in a-helical content. The difference spectrum shows also a positive band at 236 nm, which might originate from contributions of phenylalanine side chains. Zn^{2+} addition (line with squares) leads like Ca^{2+} to a decrease at 222 nm. Addition of Ca^{2+} and Zn^{2+} (line with triangles) causes the strongest decrease at 222 nm corresponding to an increase in α-helical content of S100B homodimer by about 4 residues.

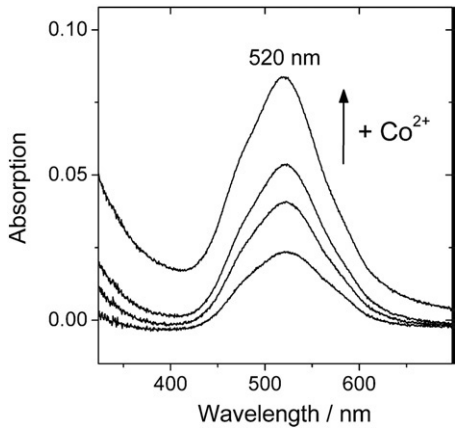

Fig. 5. $Co^{2\pm}$ binding to S100B. The Zn^{2+}-binding site in Ca^{2+}-free S100B was probed with Co^{2+}. The spectrum of Co^{2+}–S100B is in agreement with Co^{2+} coordinated by nitrogen and oxygen atom in a distorted tetraeder.

in the EF-hands provide octahedral coordination by oxygen atoms, which are not well suited for Zn^{2+} binding, that prefers tetrahedral or pentahedral coordination by nitrogen or sulfur. Recently, Moroz et al. succeeded in structure determination of Zn^{2+}-only-loaded S100A12 by X-ray crystallography revealing a conformation resembling an intermediate conformation between apo and Ca^{2+}-loaded state of S100A12 [24].

In order to characterize the Zn^{2+}-binding sites in S100B in the absence of Ca^{2+}, Co^{2+} was used as a spectroscopic probe. Addition of Co^{2+} to apo-S100B resulted in an increase in absorption with a maximum at 520 nm and a shoulder around 260 nm (Fig. 5). The absorption band centered at 520 nm is due to d–d– transitions of the Co^{2+}, which are sensitive to the coordination geometry and nature of ligand [55]. The location of the maximum suggests a mixed coordination sphere of nitrogen and oxygen ligands, whereas the shoulder around 260 nm is most likely due to nitrogen → Co^{2+} charge transfer bands. The extinction coefficient of the band centered at 520 nm of ca. 200 M^{-1} cm^{-1} is in agreement with coordination by more than four ligands in distorted tetrahedral or trigonal–bipyramidal coordination and fits well to the observed Zn^{2+}-binding site at pH 6.5 or pH 10 with three His and one Glu as ligands.

In the crystal structures of Zn^{2+}–Ca^{2+}vS100B, helix IV is slightly straightened compared to Ca^{2+}–S100B (Fig. 3A). This straightening is result from a movement of His85 and Glu89/His90 to coordinate Zn^{2+} at the dimer interface. Thereby the residues Phe87 and Phe88 are shifted by 2 to 6 Å (positions of Cα) towards the target-binding cleft of S100B. This rearrangement induced by Zn^{2+} binding might explain the observed increased binding affinity of Zn^{2+}–Ca^{2+}–S100B towards target peptides like TRTK-12 [29], which interacts with Phe87 [56, 62]. Phe87 is also involved in interactions with peptides derived from p53 [58] or NDR-kinase [63]. Positioning of Phe87 and Phe88 as observed in the structures of Zn^{2+}–Ca^{2+}–S100B in this study might also increase the affinity of S100B towards further target proteins.

Showing that Zn^{2+} already induces changes similar to those triggered by Ca^{2+} binding opens the question whether Zn^{2+} alone might also act as signaling ion via S100B. Previous studies showed that Zn^{2+}–S100B induced disassembly of microtubules and inhibited phosphorylation of τ protein by protein kinase [10,55]. Zn^{2+}-dependent interaction of S100B was also shown with IQGAP1 [31], which regulates cell morphology and motility. The results obtained here suggest that C-terminus of Zn^{2+}–S100B might form a target-binding site, which is sufficient for binding of some proteins.

2.5. Effect of Zn^{2+} binding on Ca^{2+} binding to EF-hands

Since Zn^{2+} binding to S100B leads to a 10-fold increase in Ca^{2+} affinity [27], we examined the EF-hands for conformational changes induced by Zn^{2+} binding. Interestingly, Zn^{2+}-coordinating His25 resides in the S100-specific EF-hand loop and might play a key role in the change of Ca^{2+} affinity. Structural alignments of the Zn^{2+}–Ca^{2+}–S100B with Ca^{2+}–S100B showed neither notables differences in the conformation of the N-terminal S100-specific EF-hand loop (Fig. 6B, C) nor in the classical C-terminal EF-hand loop. The positions of the Ca^{2+} ions and Ca^{2+}–oxygen bond distances are virtually identical to those in Ca^{2+}–S100B. Thus, the coordination geometry for Ca^{2+} is already optimal in the absence of $Zn^{2+}$and the binding of Zn^{2+} does not increase Ca^{2+} affinity by changes in the conformation of the Ca^{2+}-binding loops. This is further supported by structural studies on S100A12 in the Ca^{2+}- and Cu^{2+}–Ca^{2+}-loaded state [20,59]. Likewise S100B, Zn^{2+} binding to S100A12 increases the Ca^{2+} affinity [60]. In S100A12, His25 is replaced by Asp25, which is involved in Cu^{2+}/Zn^{2+} coordination. Structural alignments of the EF-hands of Cu^{2+}–Ca^{2+}–S100A12, Ca^{2+}–S100A12, and Zn^{2+}–Ca^{2+}–S100B showed that in both proteins, the EF-hand loops adopt the same conformation (Fig. 6C). We therefore concluded that Zn^{2+} binding might lead to structural changes that facilitate Ca^{2+} binding in the observed optimal geometry.

We have shown previously that, in the structure of apo-S100A2, a Na^{+} resides in the S100-specific EF-hand [61]. Similarly, a Na^{+} ion was detected in the apo-structure of S100A12 [24], suggesting that at low intracellular Ca^{2+} levels, the S100-specific EF-hand is occupied by Na^{+}. The Na^{+} ion is coordinated mainly by backbone carbonyls and proposed to stabilize the apo-state, i.e., disturbing the Na^{+} coordination might facilitate Ca^{2+} binding. In S100B, one carbonyl for Na^{+} coordination would be provided by residue His25 involved in Zn^{2+} coordination. Binding of Zn^{2+} to S100B via the sidechain of His25

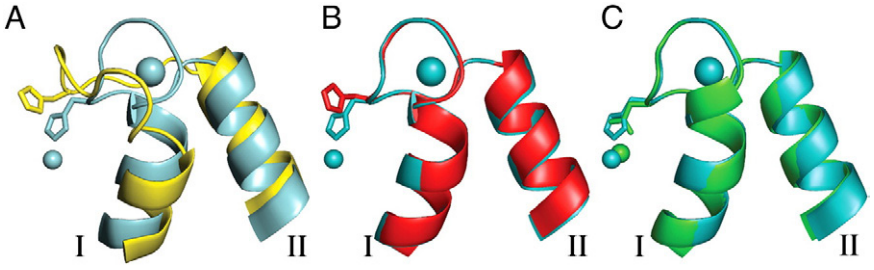

Fig. 6. Comparison of conformations of the N-terminal EF-hand in different metal–ion loaded states of S100B. (A) Comparison of the N-terminal EF-hand of Zn^{2+}–Ca^{2+}–S100B (cyan) with apo-S100B (yellow; pdb code 1B4C), (B) with human Ca^{2+}–S100B(red; pdb code 2 H61) and (C) with Cu^{2+}–Ca^{2+}–S100A12 (green; pdb code 1ODB). Ions are shown as spheres; Ca^{2+}, as large spheres; Zn^{2+} and Cu^{2+}, as smaller spheres. His25 of S100B and Asp25 of S100A12 are shown in stick type. (A) The structural alignment illustrates that, in apo-S100B, His25 is already close to the position in the Zn^{2+}–Ca^{2+}-loaded state. Zn^{2+}-binding might induce structural changes in the Ca^{2+}-binding loop, which facilitate subsequent Ca^{2+} binding leading to the observed increase in Ca^{2+} affinity. (B) The structural alignment of Zn^{2+}–Ca^{2+}–S100B (cyan) with Ca^{2+}–S100B (red) shows that His25 side chain moves towards the Zn^{2+} ion bound to S100B. The conformation of the Ca^{2+} loop is not changed. (C) Similarly, there is no change in the conformation of the Ca^{2+}-binding loop in Cu^{2+}–Ca^{2+}–S100A12 (green), indicating that the loop conformation is already optimal for Ca^{2+} binding.

(Fig. 6B) might distort the coordination of Na^+ and thereby facilitate Ca^{2+} binding. Another mechanism for increasing Ca^{2+} affinity might be the stabilization of helix IV due to the coordination of Zn^{2+} by His85′ and Glu89′/His90′. In S100 proteins, Ca^{2+} binding provides the energy for solvent exposure of hydrophobic residues in the target-binding site formed by residues of helix III, the connecting hinge loop, and the C-terminal part of helix IV. Zn^{2+} binding might reduce the required energy by helix IV stabilization, which leads in turn to a higher Ca^{2+} affinity.

2.6. PEG molecules in target-binding site

In the structures of Zn^{2+}–Ca^{2+}–S100B crystallized at pH 6.5 and pH 10.0, a fragment of a PEG molecule present in the crystallization buffer was resolved in the crystal structure. Both crystallization buffers contained PEG5000MME as precipitant, whereas PEG4000 was used for crystallization at pH 9.0, where no PEG molecule was detected. Noteworthy, the PEG molecule bound at the C-terminus of the protein (Fig. 7). In both structures, the position of the PEG molecule displays hydrophobic interactions with Phe42B, Phe87B, and Phe88B. Moreover, two oxygen atoms of PEG form hydrogen bonds to the backbone carbonyl of His42B (Fig. 7). In the structure at pH 6.5 (Fig. 7B), there is a further polar bond between the carboxyl oxygen of Glu45 and a PEG oxygen atom. The PEG molecule is further stabilized in both structures by hydrophobic interactions with His42A′ and Phe43A′ of a neighboring S100B molecule in the crystal. Crystal packing of Zn^{2+}–Ca^{2+}–S100B at pH 6.5 and 10.0 in space group $P2_1$ is related to the packing of Zn^{2+}–Ca^{2+}–S100B at pH 9.0 in space group $C222_1$due to the molecular twofold axis of the dimer, which is a true crystallographic axis in the structure at pH 9. Despite that fact, Zn^{2+}–Ca^{2+}–S100B crystallized at pH 9.0 exhibits no binding of PEG. Interestingly, Phe87 and Glu45 are essential for binding of peptides derived of target proteins such as TRTK-12 [57,62] and NDR kinase [63]. The binding of PEG to the C-terminus in the crystal structures of Zn^{2+}–Ca^{2+}–S100B supports our proposal that structural changes in the C-terminus are the cause for the increased target protein affinity of Zn^{2+}–Ca^{2+}–S100B versus Ca^{2+}–S100B.

In summary, the data presented here show that the Zn^{2+}-binding sites in S100B are flexible metal ion-binding sites most likely adapted to accommodate Zn^{2+} and Cu^{2+} with high affinity. Zn^{2+} binding leads to a stabilization of the C-terminal part of helix IV, which increases the binding affinity towards target peptides and might also contribute to the increase in Ca^{2+} affinity. Further structural studies on the structure of Zn^{2+}–S100B are in progress, which will help to understand how the Ca^{2+} affinity in S100 protein is regulated.

Acknowledgments

The financial support by grants the Deutsche Forschungsgemeinschaft (FR 1488/3-1 and FR 1488/5-1 to G.F.) and of the Wilhelm Sander-Stiftung (to T.O.) are gratefully acknowledged. We thank the staff at the Swiss Light Source, beamline X06SA (Villigen, Switzerland), for excellent support.

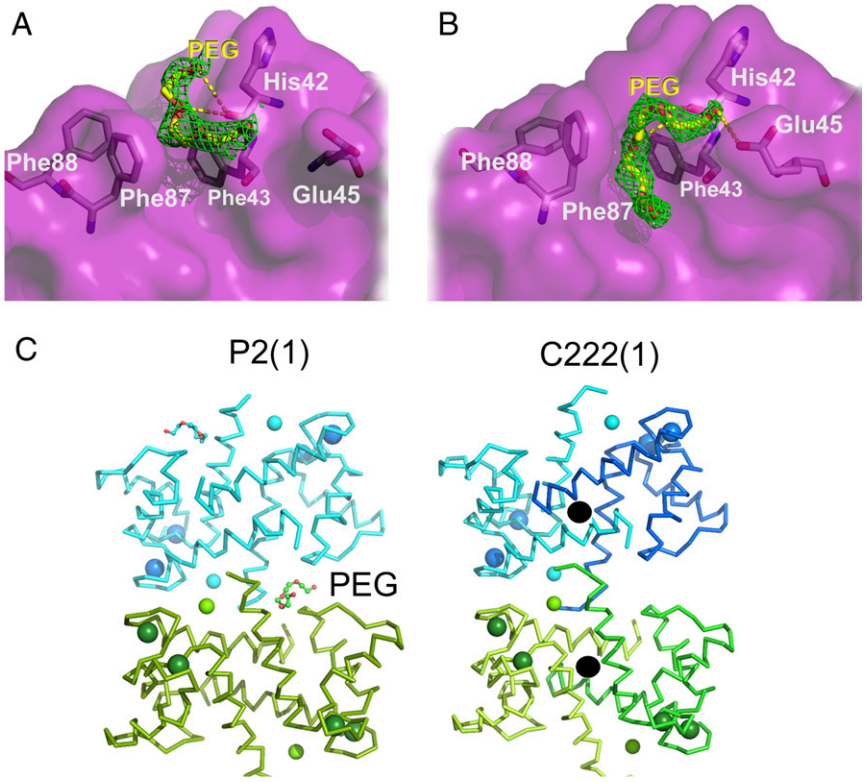

Fig. 7. PEG molecule in target-binding site of S100B. A PEG molecule was observed in the structures of Zn^{2+}–Ca^{2+}–S100B determined at pH 10 (A) and pH 6.5 (B). The PEG molecules in both structures adopt different conformations. However, the interactions with S100B are quite similar. In both structures, the PEG binding is stabilized by hydrophobic interactions with Phe43, Phe87, and Phe88, as well as by hydrogen bonds between His42 carbonyl oxygen and PEG oxygen atoms. In one structure (B), there is a further polar bond between the carboxyl oxygen of Glu45 and a PEG oxygen atom. A F_o–F_c map calculated after refinement of a coordinate file missing the PEG molecule is shown at 2.0 σ in green. (C) In the structure of Zn^{2+}–Ca^{2+}–S100B determined at pH 9.0, no PEG molecule was observed. Crystals of Zn^{2+}–Ca^{2+}–S100B at pH 9.0 belong to space group $C222_1$, whereas at pH 6.5 and pH 10 belong to space group $P2_1$. However, the packing of S100B is very similar in crystals from both space groups, since the twofold molecular axis of S100B dimer is a crystallographic axis in Zn^{2+}–Ca^{2+}–S100B crystals of space group $C222_1$. On the left-hand side, a Cα-ribbon of side Zn^{2+}–Ca^{2+}–S100B determined at pH 10 (green) and a symmetry-related molecule (cyan) is shown; Ca^{2+} and Zn^{2+} ions are shown as spheres. Right-hand side depicts Zn^{2+}–Ca^{2+}–S100B determined at pH 9 and three symmetry-related molecules. The position of the twofold crystallographic and molecular axis is perpendicular to the figure plane and indicated as a black circle.

References

[1] I. Marenholz, C.W. Heizmann, G. Fritz, S100 proteins in mouse and man: from evolution to function and pathology (including an update of the nomenclature), Biochem. Biophys. Res. Commun. 322 (2004) 1111–1122.

[2] I. Marenholz, R.C. Lovering, C.W. Heizmann, An update of the S100 nomenclature, Biochim. Biophys. Acta 1763 (2006) 1282–1283.

[3] T. Ostendorp, E. Leclerc, A. Galichet, M. Koch, N. Demling, B. Weigle, C.W. Heizmann, P.M. Kroneck, G. Fritz, Structural and functional insights into RAGE activation by multimeric S100B, EMBO J. 26 (2007) 3868–3878.

[4] C. Scotto, J.C. Deloulme, D. Rousseau, E. Chambaz, J. Baudier, Calcium and S100B regulation of p53-dependent cell growth arrest and apoptosis, Mol. Cell. Biol. 18 (1998) 4272–4281.

[5] D.B. Zimmer, L.J. Van Eldik, Analysis of the calcium-modulated proteins, S100 and calmodulin, and their target proteins during C6 glioma cell differentiation, J. Cell Biol. 108 (1989) 141–151.

[6] D.B. Zimmer, L.J. Van Eldik, Identification of a molecular target for the calcium-modulated protein S100. Fructose-1,6-bisphosphate aldolase, J. Biol. Chem. 261 (1986) 11424–11428.

[7] D.B. Zimmer, J.G. Dubuisson, Identification of an S100 target protein: glycogen phosphorylase, Cell Calcium 14 (1993) 323–332.

[8] T.A. Millward, C.W. Heizmann, B.W. Schäfer, B.A. Hemmings, Calcium regulation of Ndr protein kinase mediated by S100 calcium-binding proteins, EMBO J. 17 (1998) 5913–5922.

[9] J. Baudier, C. Delphin, D. Grunwald, S. Khochbin, J.J. Lawrence, Characterization of the tumor suppressor protein p53 as a protein kinase C substrate and a S100B-binding protein, Proc. Natl Acad. Sci. USA 89 (1992) 11627–11631.

[10] J. Baudier, R.D. Cole, Interactions between the microtubule-associated tau proteins and S100B regulate tau phosphorylation by the Ca^{2+}/calmodulin-dependent protein kinase II, J. Biol. Chem. 263 (1988) 5876–5883.

[11] G.E. Davey, P. Murmann, C.W. Heizmann, Intracellular Ca^{2+} and Zn^{2+} levels regulate the alternative cell density-dependent secretion of S100B in human glioblastoma cells, J. Biol. Chem. 276 (2001) 30819–30826.

[12] R.H. Selinfreund, S.W. Barger, W.J. Pledger, L.J. Van Eldik, Neurotrophic protein S100 beta stimulates glial cell proliferation, Proc. Natl Acad. Sci. USA 88 (1991) 3554–3558.

[13] H.J. Huttunen, J. Kuja-Panula, G. Sorci, A.L. Agneletti, R. Donato, H. Rauvala, Coregulation of neurite outgrowth and cell survival by amphoterin and S100 proteins through receptor for advanced glycation end products (RAGE) activation, J. Biol. Chem. 275 (2000) 40096–40105.

[14] W.S. Griffin, J.G. Sheng, J.E. McKenzie, M.C. Royston, S.M. Gentleman, R.A. Brumback, L.C. Cork, M.R. Del Bigio, G.W. Roberts, R.E. Mrak, Life-long over-expression of S100β in Down's syndrome: implications for Alzheimer pathogenesis, Neurobiol. Aging 19 (1998) 401–405.

[15] W.S. Griffin, L.C. Stanley, C. Ling, L. White, V. MacLeod, L.J. Perrot, C.L. White III, C. Araoz, Brain interleukin 1 and S-100 immunoreactivity are elevated in Down syndrome and Alzheimer disease, Proc. Natl Acad. Sci. USA 86 (1989) 7611–7615.

[16] R. Harpio, R. Einarsson, S100 proteins as cancer biomarkers with focus on S100B in malignant melanoma, Clin. Biochem. 37 (2004) 512–518.

[17] M. Koch, S. Bhattacharya, T. Kehl, M. Gimona, M. Vasak, W. Chazin, C.W. Heizmann, P.M. Kroneck, G. Fritz, Implications on zinc binding to S100A2, Biochim. Biophys. Acta 1773 (2007) 457–470.

[18] G. Fritz, C.W. Heizmann, P.M. Kroneck, Probing the structure of the human Ca^{2+}- and Zn^{2+}-binding protein S100A3: spectroscopic investigations of its transition metal ion complexes, and three-dimensional structural model, Biochim. Biophys. Acta 1448 (1998) 264–276.

[19] G. Fritz, P.R. Mittl, M. Vasak, M.G. Grutter, C.W. Heizmann, The crystal structure of metal-free human EF-hand protein S100A3 at 1.7-A resolution, J. Biol. Chem. 277 (2002) 33092–33098.

[20] O.V. Moroz, A.A. Antson, S.J. Grist, N.J. Maitland, G.G. Dodson, K.S. Wilson, E. Lukanidin, I.B. Bronstein, Structure of the human S100A12–copper complex: implications for host–parasite defence, Acta Crystallogr. D Biol. Crystallogr. 59 (2003) 859–867.

[21] A.J. Fielding, S. Fox, G.L. Millhauser, M. Chattopadhyay, P.M. Kroneck, G. Fritz, G.R. Eaton, S.S. Eaton, Electron spin relaxation of copper(II) complexes in glassy solution between 10 and 120 K, J. Magn. Reson. 179 (2005) 92–104.

[22] C.W. Heizmann, J.A. Cox, New perspectives on S100 proteins: a multi-functional Ca^{2+}-, Zn^{2+}- and Cu^{2+}-binding protein family, Biometals 11 (1998) 383–397.

[23] B.W. Schäfer, J.M. Fritschy, P. Murmann, H. Troxler, I. Durussel, C.W. Heizmann, J.A. Cox, Brain S100A5 is a novel calcium-, zinc-, and copper ion-binding protein of the EF-hand superfamily, J. Biol. Chem. 275 (2000) 30623–30630.

[24] O.V. Moroz, E.V. Blagova, A.J. Wilkinson, K.S. Wilson, I.B. Bronstein, The crystal structures of human S100A12 in apo form and in complex with zinc: new insights into S100A12 oligomerisation, J. Mol. Biol. 391 (2009) 536–551.

[25] D.E. Brodersen, J. Nyborg, M. Kjeldgaard, Zinc-binding site of an S100 protein revealed. Two crystal structures of Ca^{2+}-bound human psoriasin (S100A7) in the Zn^{2+}-loaded and Zn^{2+}-free states, Biochemistry 38 (1999) 1695–1704.

[26] T.H. Charpentier, P.T. Wilder, M.A. Liriano, K.M. Varney, E. Pozharski, A.D. MacKerell Jr., A. Coop, E.A. Toth, D.J. Weber, Divalent metal ion complexes of S100B in the absence and presence of pentamidine, J. Mol. Biol. 382 (2008) 56–73.

[27] J. Baudier, N. Glasser, D. Gerard, Ions binding to S100 proteins. I. Calcium- and zinc-binding properties of bovine brain S100 αα, S100a (αβ), and S100b (ββ) protein: Zn^{2+} regulates Ca^{2+} binding on S100b protein, J. Biol. Chem. 261 (1986) 8192–8203.

[28] P.T. Wilder, D.M. Baldisseri, R. Udan, K.M. Vallely, D.J. Weber, Location of the Zn^{2+}-binding site on S100B as determined by NMR spectroscopy and site-directed mutagenesis, Biochemistry 42 (2003) 13410–13421.

[29] K.R. Barber, K.A. McClintock, G.A. Jamieson Jr., R.V. Dimlich, G.S. Shaw, Specificity and Zn^{2+} enhancement of the S100B binding epitope TRTK-12, J. Biol. Chem. 274 (1999) 1502–1508.

[30] B.J. Gentil, C. Delphin, G.O. Mbele, J.C. Deloulme, M. Ferro, J. Garin, J. Baudier, The giant protein AHNAK is a specific target for the calcium- and zinc-binding S100B protein: potential implications for Ca^{2+} homeostasis regulation by S100B, J. Biol. Chem. 276 (2001) 23253–23261.

[31] G.O. Mbele, J.C. Deloulme, B.J. Gentil, C. Delphin, M. Ferro, J. Garin, M. Takahashi, J. Baudier, The zinc- and calcium-binding S100B interacts and co-localizes with IQGAP1 during dynamic rearrangement of cell membranes, J. Biol. Chem. 277 (2002) 49998–50007.

[32] P.T. Wilder, K.M. Varney, M.B. Weiss, R.K. Gitti, D.J. Weber, Solution structure of zinc- and calcium-bound rat S100B as determined by nuclear magnetic resonance spectroscopy, Biochemistry 44 (2005) 5690–5702.

[33] T. Ostendorp, C.W. Heizmann, P.M.H. Kroneck, G. Fritz, Purification, crystallization and preliminary X-ray diffraction studies on human Ca^{2+}-binding protein S100B, Acta Crystallograph. F61 (2005) 673–675.

[34] W. Kabsch, Automatic processing of rotation diffraction data from crystals of initially unknown symmetry and cell constants, J. Appl. Cryst. 26 (1993) 795–800.

[35] W. Kabsch, XDS, Acta Crystallogr. D66 (2010) 125–132.

[36] A.T. Brünger, P.D. Adams, G.M. Clore, W.L. DeLano, P. Gros, R.W. Grosse-Kunstleve, J.S. Jiang, J. Kuszewski, M. Nilges, N.S. Pannu, R.J. Read, L.M. Rice, T. Simonson, G.L. Warren, Crystallography & NMR system: a new software suite for macromolecular structure determination, Acta Crystallogr. D Biol. Crystallogr. 54 (1998) 905–921.

[37] A. Vagin, A. Teplyakov, MOLREP: an automated program for molecular replacement, J. Appl. Cryst. 30 (1997) 1022–1025.

[38] T. Ostendorp, E. Leclerc, A. Galichet, M. Koch, N. Demling, B. Weigle, C.W. Heizmann, P.M. Kroneck, G. Fritz, Structural and functional insights into RAGE activation by multimeric S100B, EMBO J. 26 (2007) 3868–3878.

[39] G.N. Murshudov, A.A. Vagin, E.J. Dodson, Refinement of macromolecular structures by the maximum-likelihood method, Acta Cryst. D53 (1997) 240–255.

[40] CCP4, The CCP4 suite: programs for protein crystallography, Acta Crystallogr. D Biol. Crystallogr. 50 (1994) 760–763.

[41] J. Painter, E.A. Merritt, Optimal description of a protein structure in terms of multiple groups undergoing TLS motion, Acta Crystallogr. D Biol. Crystallogr. 62 (2006) 439–450.

[42] A. Perrakis, R.J.H. Morris, V.S. Lamzin, Automated protein model building combined with iterative structure refinement", Nat. Struct. Biol. 6 (1999) 458–463.

[43] T.A. Jones, J.Y. Zou, S.W. Cowan, Kjeldgaard, Improved methods for building protein models in electron density maps and the location of errors in these models, Acta Crystallogr. A 47 (1991) 110–119.

[44] P. Emsley, K. Cowtan, Coot: model-building tools for molecular graphics, Acta Crystallogr. D Biol. Crystallogr. 60 (2004) 2126–2132.

[45] R.A. Laskowski, M.W. MacArthur, D.S. Moss, J.M. Thornton, PROCHECK: a program to check stereochemical quality of protein structures, J. Appl. Cryst. 26 (1993) 283–291.

[46] W.L. Delano, The PyMol Molecular Graphics System, 2002.

[47] M.M. Harding, The geometry of metal–ligand interactions relevant to proteins. II. Angles at the metal atom, additional weak metal–donor interactions, Acta Crystallogr. D Biol. Crystallogr. 56 (Pt 7) (2000) 857–867.

[48] R. Donato, Intracellular and extracellular roles of S100 proteins, Microsc. Res. Tech. 60 (2003) 540–551.

[49] C.W. Heizmann, B.W. Schäfer, G. Fritz, The family of S100 cell signaling proteins, in: R. Bradshaw, E. Dennis (Eds.), Handbook of Cell Signaling, Elsevier Science, San Diego, 2003.

[50] N. Greenfield, G.D. Fasman, Computed circular dichroism spectra for the evaluation of protein conformation, Biochemistry 8 (1969) 4108–4116.

[51] S.M. Gagne, S. Tsuda, M.X. Li, M. Chandra, L.B. Smillie, B.D. Sykes, Quantification of the calcium-induced secondary structural changes in the regulatory domain of troponin-C, Protein Sci. 3 (1994) 1961–1974.

[52] J. Baudier, D. Gerard, Ions binding to S100 proteins: structural changes induced by calcium and zinc on S100a and S100b proteins, Biochemistry 22 (1983) 3360–3369.

[53] W.H. Yu, P.E. Fraser, S100beta interaction with tau is promoted by zinc and inhibited by hyperphosphorylation in Alzheimer's disease, J. Neurosci. 21 (2001) 2240–2246.

[54] J. Baudier, C. Holtzscherer, D. Gerard, Zinc-dependent affinity chromatography of the S100b protein on phenyl-Sepharose. A rapid purification method, FEBS Lett. 148 (1982) 231–234.

[55] I. Bertini, C. Luchinat, High spin cobalt(II) as a probe for the investigation of metalloproteins, Adv. Inorg. Biochem. 6 (1984) 71–111.

[56] K.A. McClintock, L.J. Van Eldik, G.S. Shaw, The C-terminus and linker region of S100B exert dual control on protein–protein interactions with TRTK-12, Biochemistry 41 (2002) 5421–5428.

[57] K.G. Inman, R. Yang, R.R. Rustandi, K.E. Miller, D.M. Baldisseri, D.J. Weber, Solution NMR structure of S100B bound to the high-affinity target peptide TRTK-12, J. Mol. Biol. 324 (2002) 1003–1014.

[58] R.R. Rustandi, D.M. Baldisseri, D.J. Weber, Structure of the negative regulatory domain of p53 bound to S100B(betabeta), Nat. Struct. Biol. 7 (2000) 570–574.

[59] O.V. Moroz, A.A. Antson, G.N. Murshudov, N.J. Maitland, G.G. Dodson, K.S. Wilson, I. Skibshoj, E.M. Lukanidin, I.B. Bronstein, The three-dimensional structure of human S100A12, Acta Crystallogr. D Biol. Crystallogr. 57 (2001) 20–29.

[60] E.C. Dell'Angelica, C.H. Schleicher, J.A. Santome, Primary structure and binding properties of calgranulin C, a novel S100-like calcium-binding protein from pig granulocytes, J. Biol. Chem. 269 (1994) 28929–28936.
[61] M. Koch, J. Diez, G. Fritz, Crystal structure of Ca^{2+} -free S100A2 at 1.6 resolution, J. Mol. Biol. 378 (2008) 931–940.
[62] K.A. McClintock, G.S. Shaw, A novel S100 target conformation is revealed by the solution structure of the Ca^{2+}–S100B–TRTK-12 complex, J. Biol. Chem. 278 (2003) 6251–6257.
[63] S. Bhattacharya, E. Large, C.W. Heizmann, B. Hemmings, W.J. Chazin, Structure of the Ca^{2+}/S100B/NDR kinase peptide complex: insights into S100 target specificity and activation of the kinase, Biochemistry 42 (2003) 14416–14426.
[64] H. Matsumura, T. Shiba, T. Inoue, S. Harada, Y. Kai, A novel mode of target recognition suggested by the 2.0 Å structure of holo S100B from bovine brain, Structure 6 (1998) 233–241.
[65] W. Kabsch, C. Sander, Dictionary of protein secondary structure: pattern recognition of hydrogen-bonded and geometrical features, Biopolymers 22 (1983) 2577–2637.